Identifying topographic changes at the beach using multiple years of permanent laser scanning

Kuschnerus, Mieke; de Vries, Sierd; Antolínez, José A.Á.; Vos, Sander; Lindenbergh, Roderik

DOI
10.1016/j.coastaleng.2024.104594

Publication date
2024

Document Version
Final published version

Published in
Coastal Engineering

Citation (APA)
Kuschnerus, M., de Vries, S., Antolínez, J. A. Á., Vos, S., & Lindenbergh, R. (2024). Identifying topographic changes at the beach using multiple years of permanent laser scanning. *Coastal Engineering*, *193*, Article 104594. https://doi.org/10.1016/j.coastaleng.2024.104594

Coastal Engineering 193 (2024) 104594

Contents lists available at ScienceDirect

Coastal Engineering

journal homepage: www.elsevier.com/locate/coastaleng

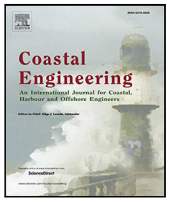

Identifying topographic changes at the beach using multiple years of permanent laser scanning

Mieke Kuschnerus [a,*], Sierd de Vries [b], José A.Á. Antolínez [b], Sander Vos [b], Roderik Lindenbergh [a]

[a] Department of Geoscience and Remote Sensing, Delft University of Technology, Stevinweg 1, Delft, 2628CN, The Netherlands
[b] Department of Hydraulic Engineering, Delft University of Technology, Stevinweg 1, Delft, 2628CN, The Netherlands

ARTICLE INFO

Dataset link: http://dx.doi.org/10.4121/1aac46fb-7900-4d4c-a099-d2ce354811d2.v2

Keywords:
Laser scanning
LIDAR
Aeolian sand transport
Anthropogenic influences
Multi-temporal 3D point cloud analysis
Permanent laser scanning
Change detection

ABSTRACT

Sandy beach-dune systems make up a large part of coastal areas world wide. Their function as an eco-system as well as a protective barrier for human and natural habitat is under increased threat due to climate change. A thorough understanding of change processes at the sediment surface is essential to facilitate prediction of future development and management strategies to maintain their function. Especially slow and small scale processes happening over several days up to weeks at cm level, such as aeolian sand transport are difficult to identify and analyse. Permanent laser scanning (PLS) is a useful tool in the study and analysis of coastal processes as it captures a data representation of the evolution of the sediment surface over extended periods of time (up to several years) with high detail (at cm-dm level). The PLS data set considered for this study, consists of hourly acquired 3D point clouds representing the surface evolution of a section of the Dutch coast during three years. However, it is challenging to extract concrete information on specific change processes from the large and complex PLS data set. We use multiple hypothesis testing in order to reduce the PLS data set to a so-called inventory of trends, consisting of 12.8 million partial time series with associated rate of change and elevation. The inventory of trends proofs to be a suitable tool to identify natural processes such as storms and aeolian sand transport in our test area in the aeolian zone of a sandy beach-dune system on the Dutch coast. We identify these processes and provide a tool to derive summarising data from the complex PLS data set. We find that all partial time series identified as most likely representing aeolian sand transport, result in 1354 m^3 of sand deposition in our study area over the course of three years. We also show a comparison with transects from JarKus data and find a correlation between anthropogenic activities and erosion in our test area with a correlation coefficient of 0.3.

1. Introduction

Coastal areas worldwide serve a multitude of purposes. Specifically sandy beach-dune systems (SBDS), which make up 31% of non-iced coast (Luijendijk et al., 2018), serve as a protective barrier to prevent flooding, as habitat for a large number of species, and as recreational areas. The resilience of SBDS is under increasing pressure due to both natural and human driven climate change (Intergovernmental Panel on Climate Change (IPCC), 2014; Grabemann and Weisse, 2008). While sea level rise and increased severity of storm events are foreseen, the growing human population continues to develop infrastructure on and near coastal areas worldwide, which under improvisational planning can lead to coastal squeeze (Vousdoukas et al., 2020). To mitigate these effects, predictions of the development of SBDS are needed, which require a thorough understanding of topographic changes at the sediment surface of SBDS.

Topographic coastal changes at SBDS are driven by anthropogenic, ecologic and geomorphological processes at different spatial and temporal scales. These driving influences also interact. While a storm can cause significant erosion of the beach-dune profile over the course of several hours (van Wiechen et al., 2023), wind driven sediment transports may only cause significant accretion of the dune profile of comparable extent over the course of several decades (de Vries et al., 2012). In addition, the net result of the interaction between erosive and accretive processes is sensitive to even small changes in any of the influencing factors (Stive et al., 2002). Thus, human interventions, like shore nourishment, frequent beach maintenance or buildings on the beach might influence these as well (Schipper et al., 2016; Poppema et al., 2021). The knowledge needed to analyse past and present development in order to make viable predictions of the future, can be gained by observing, quantifying and subsequently interpreting these

* Corresponding author.
E-mail address: m.kuschnerus@tudelft.nl (M. Kuschnerus).

https://doi.org/10.1016/j.coastaleng.2024.104594
Received 21 December 2023; Received in revised form 21 June 2024; Accepted 8 August 2024
Available online 10 August 2024

dynamics and interactions at the sediment surface at different time scales.

Given the difference in scale, processes and interactions may be challenging to identity and analyse through sparse observations of surface beach dynamics. Regular and frequent observations at high level of detail are desired to cover all temporal and spatial scales. Optical as well as radar remote sensing are suitable observation tools, as well as in-situ measurements with sensors and through inspections.

Yearly observation of the Dutch coast with airborne laser scanning provide a tool to monitor the long term development of surface dynamics in the Dutch beach-dune system. The resulting JarKus transects (Rijkswaterstaat - Dutch Ministery of Infrastructure and Water Management, 2022) were for example analysed by van IJzendoorn et al. (2021). These transects, regularly spaced at 250 m, are used to study the location of the coastline (quantified as momentary coastline (MKL)) and for decision making in coastal management in the Netherlands.

Several other studies use incidental terrestrial laser scanning to observe the effect of one specific event or process (see for example Ackerley et al., 2016; Schubert et al., 2015). Permanent laser scanning is a tool to continuously monitor a section of coast over a longer period at high temporal frequency (up to hourly) and small spatial resolution (up to cm) (see Vos et al., 2017; Anders et al., 2019). Permanent laser scanning has been used in combination with analysis of video images to detect bulldozer activities on the beach (Barbero-García et al., 2023) and for several other applications, for example glacier observation (Voordendag et al., 2021) and rock fall monitoring (Schröder et al., 2022).

Anders et al. (2019) developed the so-called 4D-objects by change to find spatially connected areas in which time series behave in a similar way. Each 4D object by change can then be associated with a physical process, that would typically cause this pattern. Their method favours prominent changes and only finds affected areas that are connected, like for example bulldozer works or the appearance of a sand bar. A method to group and classify the 4D-objects by change was developed by Hulskemper et al. (2022). In our previous study on a similar data set of shorter length (covering six months), we used clustering algorithms to group time series with similar change behaviour to identify areas affected by the same physical processes (Kuschnerus et al., 2021). This method turned out to be useful for finding areas affected by bulldozer works as well as different erosion rates in the intertidal area. However, it is less suitable to process our entire three year data set. Winiwarter et al. (2023) used Kalman filtering to process long time series containing gaps and found those time series to be a suitable input to feature based clustering methods.

The aim of this paper is to identify topographic changes at the sediment surface of the beach-dune system using permanent laser scanning on a section of the Dutch coast. The permanently installed instrument measures with high frequency (hourly) and covers a section of about 800 m length in high detail (cm to dm level of elevation change). The acquired data set captures the surface dynamics but its structure of 3D point clouds is cumbersome and information is not easily extracted. We propose a method to extract elevation time series and their rates of change and collect them as an *inventory of trends* in order to reduce and simplify the data set. The trend inventory allows to identify and analyse observed dynamics over a period of three years. We demonstrate the link but also the additional value compared to the JarKus data set by relating the observations in the respective matching locations. Specifically we aim to answer the following research questions:

1. What elevation trends at the sediment surface can be derived from the PLS data set?
2. How do high resolution PLS data compare to yearly JarKus-data?
3. How can small and slow changes at the sediment surface be identified and quantified with PLS?
4. How can the effect of anthropogenic activities on the dynamics at the sediment surface be analysed using PLS data?

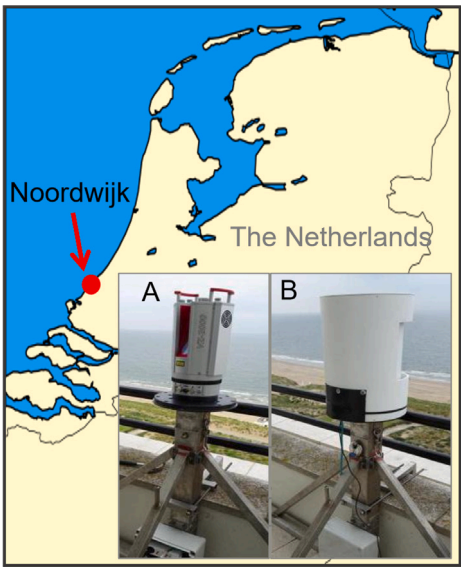

Fig. 1. The study site on the Dutch coast in Noordwijk, The Netherlands with the laser scanner mounted on a hotel balcony without (A) and with (B) protective cover.

The novelty of the proposed work is, firstly, the presented method to generate a simpler representation of our data set for efficient data mining. Secondly, we process for the first time the entire hourly three-year data record from permanent laser scanning, which has proven to be challenging with previously developed methods. Finally, our methods allow to identify surface dynamics in the aeolian zone, which are difficult to study with other types of data and methods (see for instance Uphues et al., 2022). Especially our new method is capable of capturing long term but small-scale changes due to aeolian sand transport.

2. Field site and data set

The study area is part of a typical example of a Dutch urban beach and provides the infrastructure needed for the instrumental set-up. The Dutch beach-dune system is orientated from south-southwest to north-northeast and consists of quarts sand (van IJzendoorn et al., 2023). The coast is driven by meso-tidal tides of about 2 m height (Wijnberg, 2002), waves of about 1.7 m height during average conditions and 5 m height during storm conditions (Luijendijk et al., 2017) and with south westerly winds (Vos et al., 2024). The Dutch coast is maintained regularly (Maij-Weggen, 1990) with (underwater) sand nourishments resulting in an accreting environment around Noordwijk (de Vries et al., 2012). The observed area includes a sandy beach and dunes, covered with vegetation and is about 1 km long and 250 m wide. The beach varies in width between 80 m and 140 m under normal weather conditions. In rare occasions, storm reduces the width of the beach even further. Fig. 2 shows an overview of the study area with an aerial image and the top view of a point cloud as an example. In the point cloud the colours are based on elevation. We focus in this study on a 400 m long part of the aeolian zone and do not include the intertidal zone or dunes. Within the study area there is often a beach scarp of up to 1 m height, see Fig. 2B, which can lead to sudden changes in elevation observations.

To identify and analyse change processes, we use an exemplary data set from permanent lasers scanning (PLS) consisting of point clouds collected hourly during a period of three years from July 2019 to June 2022. The entire data set is published and can be accessed through 4TU.ResearchData (Vos et al., 2023). A summary of parameters describing the data set can be found in table Table 1. The point clouds processed for this study are acquired with a Riegl VZ-2000 laser scanner, which is permanently mounted on the balcony of Grand Hotel

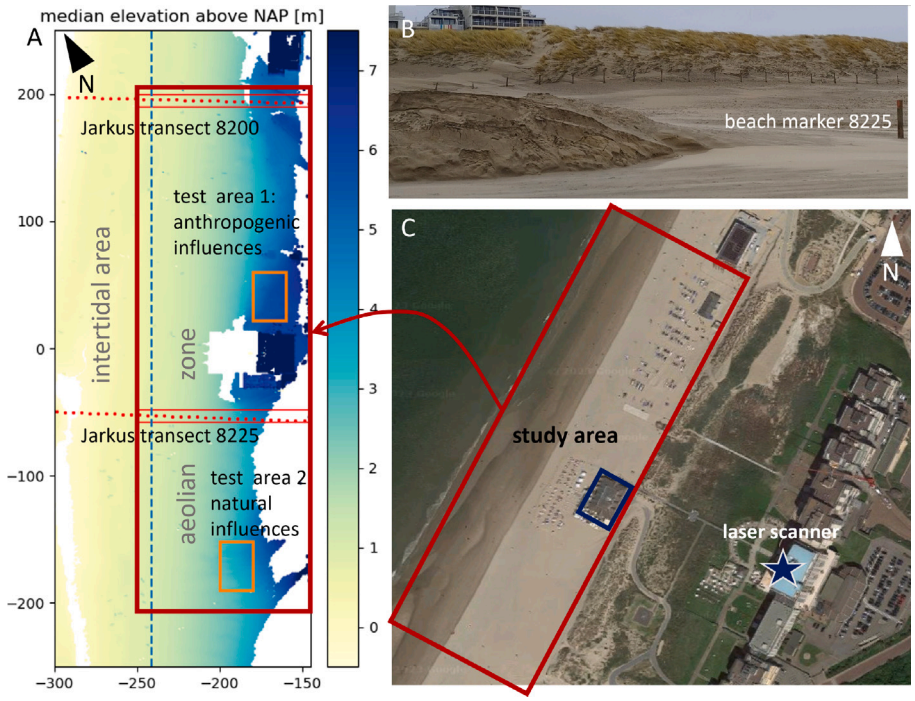

Fig. 2. Overview of study area: Point cloud of the sandy beach (A), photo of a beach scarp formed at the edge of the aeolian zone (B) and aerial image of Grand Hotel Huis ter Duin with the adjacent dunes and beach (C, by Google maps). In the point cloud the colours are based on elevation. White areas appear because of missing data in the point clouds in the shadow zones of dunes and buildings, or because of water present in the intertidal zone. The test areas are marked with a square: test area 1 is next to a beach cafe and influenced by many anthropogenic changes (i.e. bulldozer works, frequent visitors) and test area 2 is mostly influenced by natural processes. In photo (B) the beach marker at location of Jarkus transect with ID 8225 is visible. The location of the laser scanner is marked with a star in the aerial image.

Table 1
Data properties considering all hourly scans between 11 July 2019 and 21 June 2022.

Total number of files	20 875
Number of good quality files	19 386
Days scanned	954
Interruptions (>24 h)	21
Number of points in study area	800 000
Range	145–500 m
Point density	1–40 pt/m^2
Footprint size	0.02–0.1 m^2
Inclination angle	70–90 deg

Table 2
Specifications of Riegl VZ-2000 laser scanner according to documentation.

Range accuracy (at 150 m range) [m]	0.008
Angular spacing [deg]	0.003
Beam divergence [mrad]	0.3
Inclination sensor frequency [Hz]	1
Measurement accuracy [deg]	0.008

Huis ter Duin in Noordwijk, The Netherlands. The laser scanner is mounted on a metal frame at 55.757 m height above NAP that is fixed to the balcony to maximise stability and covered with a protective cover (see Fig. 1).

2.1. Instrument settings

The settings of the laser scanner are summarised in Table 2. Data is collected by running a scan of nearly 180 horizontal degrees covering a stretch of beach of just under 1 km long every hour with an angular spacing of 0.03 degree.

The laser scanner generates a 3D point cloud per scan, made up of x,y,z-coordinates which are calculated by the Riegl proprietary software out of recorded range, horizontal and vertical angle data, as well as intensity of the backscatter signal, per point. The internal inclination sensor records inclination values during each scan, with a frequency of 1 Hz (not matching the scanning frequency). A mean value and the standard deviation of these inclination angles is used for correction of tilts in the scanner (see Section 3.1).

There are some temporal gaps in the data set, of which the two largest are the following: in the spring of 2020 during a period of 1.5 months the scanner underwent maintenance and was not recording while on 19th December 2021 the scanner stopped recording data unnoticed for a period of 18 days due to the holiday season (see Table 1).

The JarKus data set is collected yearly based on different measurement techniques. Every 250 m along the Dutch coast a transect is measured to determine the current beach and dune profile as well as the current position of the coastline with respect to a reference coastline. In our observation area in Noordwijk two transects (with ID 8200 and 8225) are located (see Fig. 2A). We focus our comparison on the part on the sandy beach in the aeolian zone. In this part the JarKus data is collected with airborne laser scanning. Findings on these transects, interpretation of data and summary of most relevant parameters are summarised in reports by the Dutch ministry of infrastructure and water management (Rijkswaterstaat, Rijksinstituut voor Kust en Zee, 2022). A visualisation of the trend of the momentary coastline (MKL) in 2022 is shown in Fig. 3.

Additionally data from weather stations of the Royal Netherlands Meteorological Institute Koninklijk Nederlands Meteorologisch Instituut (KNMI) (2022) in IJmuiden and Hoek van Holland is used to compare our findings to meteorological properties, such as wind speed and direction and precipitation.

3. Generation of inventory of trends

In order to simplify the 3D point clouds, we rasterize each one into a grid. Then we generate the so called *inventory of trends* out of time series at the grid locations on the beach. The resulting database of trends is

Fig. 3. Location of JarKus transects around Noordwijk in the Netherlands with current trend of MKL in 2022 as a bar plot at each transect location (Rijkswaterstaat, Rijksinstituut voor Kust en Zee, 2022).

then used for further analysis of specific regions and time periods as well as to come up with overall statistics of the entire field site.

The method is explained in several steps as visualised in Fig. 4. In a first step a data set of corrected point clouds is generated from the raw data, see Section 3.1. Then, digital elevation models (DEMs) are used to derive a set of elevation time series located at regular grid points, as discussed in Section 3.2. With the help of these time series and multiple hypothesis testing (MHT) a trend inventory is built, Section 3.3, which allows then to derive the results for interpretation of natural and anthropogenic processes, compare Section 3.4.

3.1. Corrected point clouds and filtering

The laser scanner data is in a local coordinate system with the location of the laser scanner as its origin. The height of the scanner was determined when mounted with a GPS receiver. This constant elevation is added to the z-coordinate, to process actual height above sea level instead of negative elevation with respect to the scanner's location.

In a next step the inclination data from the laser scanner is averaged for each scan and the mean pitch and roll inclination are extracted. These values are then used to calculate rotation matrix R, given by:

$$R = \begin{pmatrix} \cos(\varphi) & 0 & \sin(\varphi) \\ \sin(\varphi)\cdot\sin(\theta) & \cos(\theta) & -\cos(\varphi)\cdot\sin(\theta) \\ -\sin(\varphi)\cdot\cos(\theta) & \sin(\theta) & \cos(\varphi)\cdot\cos(\theta) \end{pmatrix} \quad (1)$$

with φ the pitch angle and θ the roll angle. Rotation matrix R is calculated for each point cloud separately and applied, if the standard deviation of the pitch and roll values during the entire scan is below a threshold. This is to ensure that data that was e.g. obtained during a heavy storm is not corrected with a rotation based on erroneous inclination values. If the threshold is not met, a mean pitch and roll value based on the other scans in that month is used for correction. A constant general tilt of the point cloud is removed in this way, as well as the main part of deviations of the laser scanner's position due to temperature changes (heat expansion of supporting materials) or strong winds. We do not use any ground control points for correction of individual point clouds. For validation, some ground control points were measured at the start of data acquisition.

Subsequently the data set is filtered for low quality or erroneous point clouds. The mean elevation as well as the sum of residuals

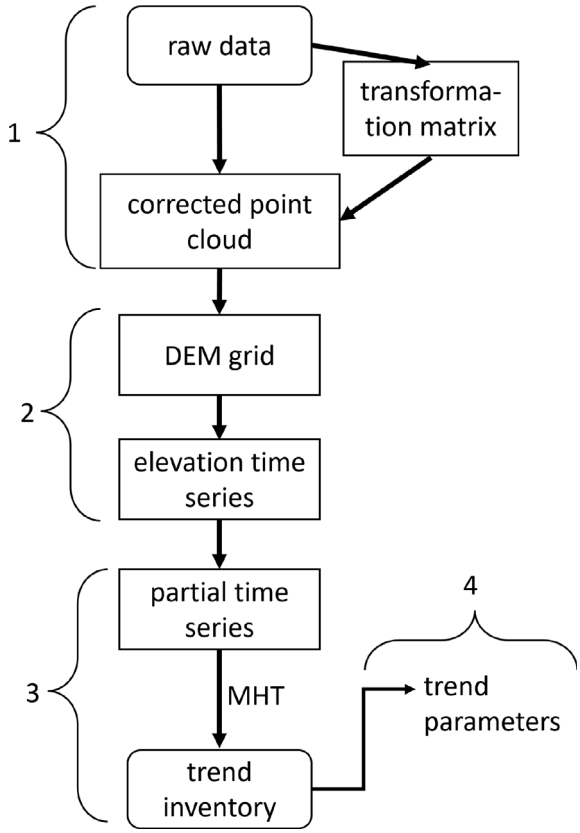

Fig. 4. Flow chart of the methodology. The numbers refer to the four data processing steps, 1: generation of corrected point cloud, 2: reformatting as elevation time series, 3: data reduction to inventory of trends and 4: Reporting of statistical trend parameters.

deviating from a fitted plane through a reference surface are estimated for each point cloud. If the mean elevation deviates more than 10 cm or the summed residuals are larger than 10 cm the point cloud is not considered for our study. This threshold was determined during a previous study, Kuschnerus et al. (2024), considering the error sources and influences on data quality. This is to exclude point clouds with large variations/noisy data caused by instrument failure or storms. Point clouds recorded during low visibility weather conditions, which do not contain data on the sandy beach, are excluded from further analysis as well. This leaves a data set of 19 386 good quality point clouds acquired between 11 July 2019 at 14:00 and 21 June 2022 12:00 (midday).

3.2. Digital elevation models and elevation time series

The corrected point clouds are then cropped to the relevant part to contain only the sandy beach. For further processing a grid of 1 m × 1 m is formed and all elevations in each grid cell are averaged to obtain an elevation at the centre of the grid cell, compare Fig. 5. The 1 m × 1 m-grid size is a common standard for analysis of coastal spatial data and models. Additionally, it was chosen in order to be as small as possible, while still containing enough points to derive statistically significant mean elevation on most locations in the study area. A sensitivity analysis on point clouds from our data set in comparison with higher resolution data at the same location was presented by Di Biase et al. (2022). The square root of the summed residuals are calculated for each grid cell:

$$\sigma_g = \sqrt{\frac{\underline{\mathbf{e}}^T\underline{\mathbf{e}}}{n_p - 1}}, \quad (2)$$

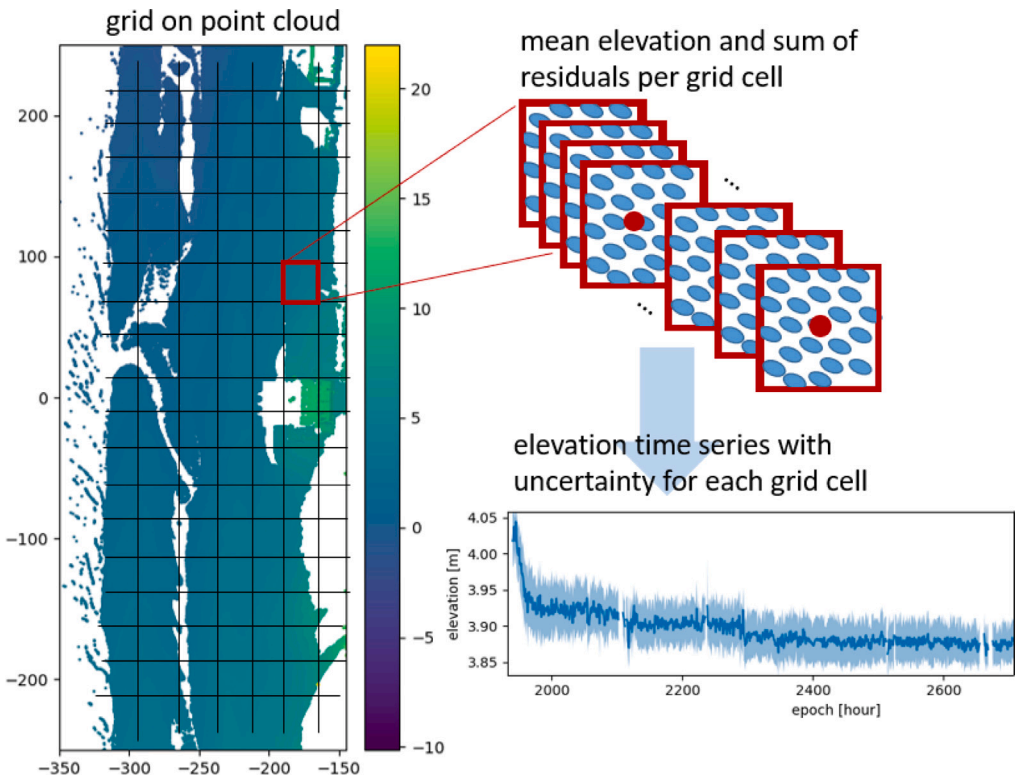

Fig. 5. Schematic of time series generation: each point cloud is divided into grid cells. For each grid cell all recorded points are summarised by mean elevation and sum of residuals. These values for all available point clouds then provide a time series of about 19 000 elevation values with associated sum of residuals for each grid cell location.

for the spatial residual vector $\underline{\mathbf{e}}$ and number of points n_p. The summed residuals are then saved for each grid cell, as well as the number of points per grid cell. Since the elevations in the DEMs are as a consequence available at regular grid points, all files that meet quality criteria are then collected to generate a time series of 19 386 epochs for each grid cell location. For each grid cell location we have the elevation time series with the mean elevation per time stamp and the accompanying uncertainty time series with the summed residuals per time stamp. Each time series may contain gaps for several reasons:

- a point cloud was not available because it was not recorded or of bad quality,
- an object or pile of sand is temporarily blocking the view on the grid cell, or,
- the tides cause the grid cell to be temporarily under water.

That last case is used to determine events, where high water reaches the study area. For every day we determined the point cloud with the narrowest beach width and save that moment of time and water line at that time as our estimation for the high water line on that day and the time of high tide. This method was described in more detail in a previous study to determine the development of the beach width (Kuschnerus et al., 2023).

3.3. 4D inventory of trends of surface elevations

Each time series is divided into partial time series. A break point is recorded when there is a gap in the time series of more than three hours or if a jump is recorded in the time series. To detect the jumps or change point the so called Pruned Exact Linear Time (PELT) algorithm is used, Killick et al. (2012). The PELT algorithm is using minus the maximum log-likelihood as a cost function and adds a point as change point, if it reduces the segmentation costs by more than a penalty term. We used the implementation of the algorithm in the *ruptures* Python package, Truong et al. (2020). This will also split partial time series with non-monotonic trends at the points where the trend changes.

After the time series is divided into partial time series we use multiple hypothesis testing (MHT) to build the 4D inventory of trends. Goal is to classify each partial time series as (i) stable, (ii) linearly increasing or decreasing, or, (iii) without matching model.

As described in detail in Kuschnerus et al. (2024) and similar to Lindenbergh and Hanssen (2003), we use MHT based on the method presented by Chang and Hanssen (2016). Chang and Hanssen (2016) use MHT to determine an appropriate deformation model for time series of kinematic parameters from InSAR data. Here, we are interested in estimating linear trends for each of the partial time series. Therefore, we choose a linear model as alternative hypothesis to the null-hypothesis. The null-hypothesis, H_0, states that there is no statistically significant change in the respective time series segment.

We first test for the null-hypothesis (i.e. no statistically significant change). If the null-hypothesis is accepted, we save the start and end of the partial time series, slope value 0 and mean elevation over the entire duration. The null-hypothesis is formulated as follows:

$$H_0 : A_0 = \begin{pmatrix} 1 \\ 1 \\ \vdots \\ 1 \end{pmatrix}, \quad x = \underline{\hat{h}} \tag{3}$$

$$T_0 \sim \chi^2(1, 0), \tag{4}$$

For model matrix A_0 and test value T_0, which is centrally χ^2-distributed with 1 degree of freedom, since we have one free parameter that is estimated. The free parameter is here the mean elevation value, $\hat{\underline{h}}$, of the time series of elevation values $\underline{h}$.

As alternative hypothesis, H_1, we consider a linear trend:

$$H_1 : A_1 = \begin{pmatrix} 1 & t_1 \\ \vdots & \vdots \\ 1 & t_m \end{pmatrix}, x = \begin{pmatrix} h_0 \\ v \end{pmatrix} \tag{5}$$

$$T_1 \sim \chi^2(1, \lambda) \tag{6}$$

where h_0 is the intercept and v the rate of change of the linear model and therefore $A_1 \in \mathbb{R}^{m\times 2}$. The test value here follows a χ^2-distribution with 1 degree of freedom and non-centrality parameter $\lambda \neq 0$, since we have a 2-dimensional model matrix and one additional free parameter compared to the null-hypothesis. The covariance matrix Q_h is defined using the RMSE per grid cell σ_g^2, which were saved for every grid cell together with the elevation time series. We assume that there is no correlation between subsequent measurements and therefore obtain the diagonal matrix

$$Q_h = \mathrm{diag}(\sigma_{g1}^2, \dots, \sigma_{gm}^2) = \underline{\sigma_g^2} \cdot I_m, \tag{7}$$

with

$$\underline{\sigma_g^2} = (\sigma_{g1}^2, \dots, \sigma_{gm}^2) \tag{8}$$

the vector of epoch dependent grid-wise variances σ_{gi}^2, for $i = 1, \dots, m$.

Following Chang and Hanssen (2016), the test value T_1 for the alternative hypotheses, is then calculated as

$$T_1 = \sum_{i=1}^{m} \frac{(h_i - \hat{h})^2}{\sigma_i^2}, \tag{9}$$

for modelled time series $\underline{\hat{h}} = A_1 \cdot \hat{x}$. The test value is then compared to the critical value k_α, determined by significance level α and non-centrality parameter λ. The chosen parameters in our case are significance level $\alpha = 0.95$ (determining a false alarm rate of 5%) and the power of the test $\gamma = 0.8$ (80% probability of missed detection). Since we are using the χ^2-distribution, the non-centrality parameter λ needs to be chosen in order to represent the significance value α and the power of the test γ. More details on the determination and influence of λ can be found in Kuschnerus et al. (2024). Here we use $\lambda = 7.85$ to represent a statistical test set up with our chosen parameters, i.e. 5% probability of detecting a trend, even though there is none, and 80% probability of detecting a trend, when one is present.

If a statistically significant trend is detected, we save the value of the trend in m/day together with the start and stop time of the partial time series and the initial elevation (estimated as axis-intercept). In this way we derive a table of start and stop times and slope values for each grid cell location.

3.4. Parameter extraction

The trend inventory delivers a database of statistically significant trends for each time step and each location in our field site. For specific questions, for example the impact of one storm, we can now zoom in on a time period and collect all available partial time series, the matching trends, and the overall change in volume. Also, specific areas can be highlighted, observed over the entire observational period as well as for shorter time spans. To get a quick look on what could have happened for different zoom-in situations (in space and/or time), we calculate the total number of partial time series, the number of partial time series with significant trends, the average duration of the partial time series with significant trends and the average rate of change from the trend inventory. Additionally we report on net volume and area change over the time period, as well as the total sum of absolute volume change. Together, these parameters provide indications on the net results of erosion and deposition processes as well as a measure of how dynamic an area has been.

4. Results

As results of our analysis we present statistics on the inventory of trends of the entire area (Section 4.1) and a comparison with transects from the JarKus data set (Section 4.2). Then we show how some commonly occurring physical processes appear in the trend inventory (Section 4.3). Finally we compare the trend inventory for an area with frequent bulldozer works with an area that is dominated by natural processes (Section 4.4).

Table 3
Summary of statistics of trend inventory. Time series is denotes as 'ts'.

Number of grid cells	41 000
Number of partial time series	12.8 million
Average duration of partial time series	45 h
Number of significant change rates	395 825
Average duration of ts with significant change rates	158 h
Max duration of ts with significant change rates	1209 h
Average change rate	0.0027 m/day
Number of stable ts	3.2 million

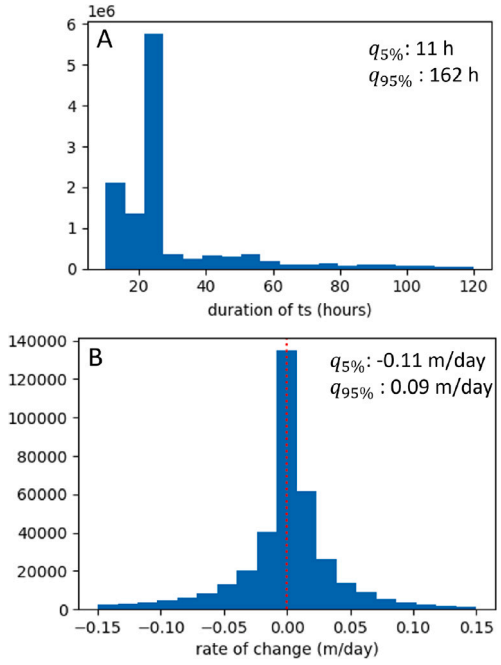

Fig. 6. Histograms of duration of partial time series (A) and of rates of change (B).

4.1. Inventory of trends

Following the above described procedure, we calculated the inventory of trends for the entire data set covering three years of hourly observations. The statistics on the entire area are listed in Table 3 together with the histogram of the rates of change in Fig. 6. We can see in the table that over the entire area of 41 000 grid cells we have 12.8 million partial time series. For a large part of those time series (about 8 million) we cannot find a statistically significant linear model. The reason for that is either that the shape of the partial time series does not fit a linear model or that the partial time series is too short or has too many gaps in order to be considered. About 3.2 million partial time series appear to represent a period of time where there is no statistically significant rate of change in elevation recorded. We also observe that the average duration of partial time series is 45 h, but the average duration of partial time series with a statistically significant trend is more than three times longer (158 h), with a maximum duration of 1209 h (about 50 days). The minimum duration for all partial time series is 10 h and was fixed as a setting in the processing.

In Fig. 7 we show a time line of all major storm events and data gaps for three example time series of raw elevation data as well as fitted linear models for the respective partial time series. The elevation at the time of the JarKus data acquisition at the corresponding location is marked with dots in the same colour as the respective time series. Occurrences of measured wind speeds of 18 m/s and higher are indicated with a yellow bar. The most prominent gaps in the time series are due to failure in data acquisition or bad quality data. Major storms during extreme wind speeds (as for example storms Ciara and Dennis in

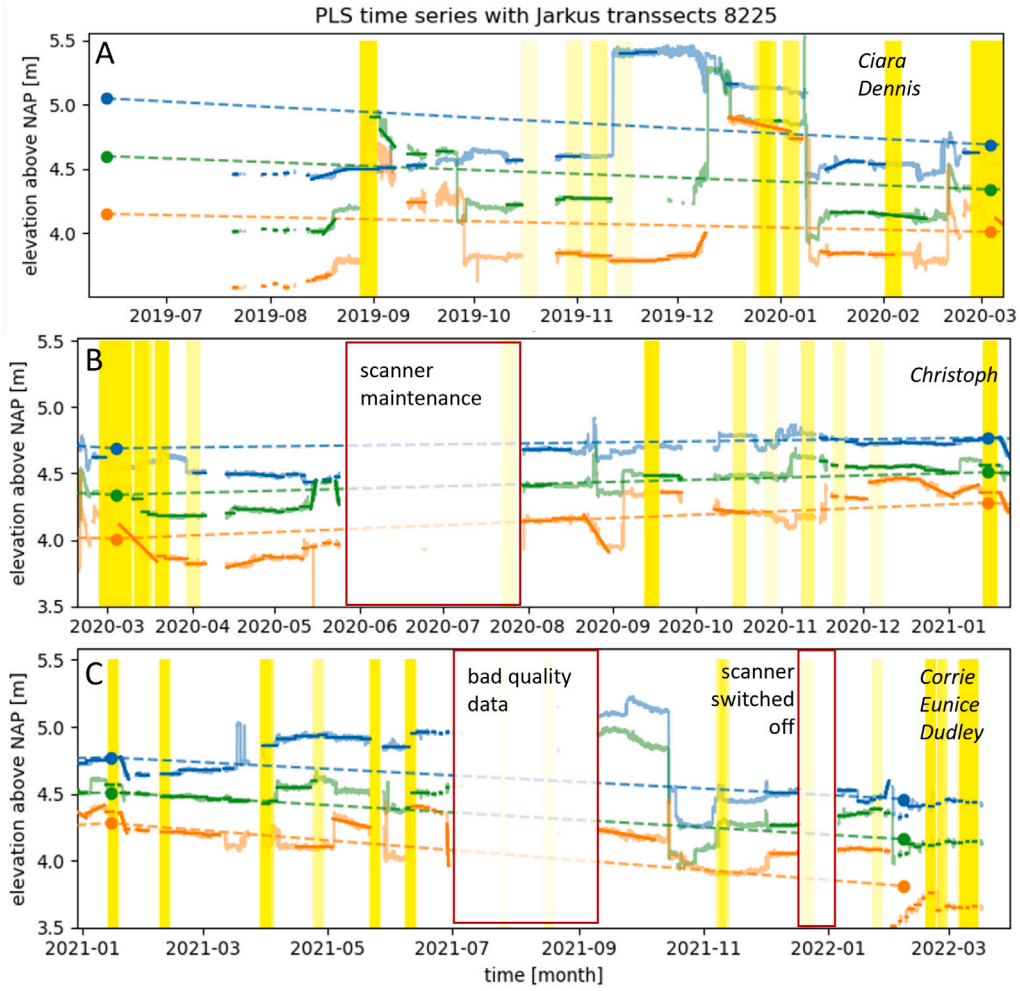

Fig. 7. Time line of data collection split up in the periods between JarKus campaigns (A: 2019/2020, B: 2020/2021, C: 2021/2022) for three example grid cells along the JarKus transect with ID 8225. JarKus data collection is indicated by a dot at the acquisition time and measured elevation of the transect. The raw elevation data is shown for three grid cells (blue, orange and green time series) along JarKus transect 8225. The fitted trends are shown in the same colour on top of the raw data. Hours with an average wind speed ≥18 m/s, are indicated by a yellow bar. The names of some prominent major storms are provided in italics and reasons for large gaps in the data are given in/next to a red box.

February 2020 and Eunice in February 2022) can be observed as well at times where there are abrupt changes or gaps. Another possible reason for sudden changes or jumps is a beach scarp that form on the beach as shown in Fig. 2B. We observe lots of dynamics (up to 1 m in elevation difference) in between two JarKus height estimates, which are missed by interpolating data from yearly measurement campaigns for JarKus.

4.2. Comparison of trend inventory with JarKus transects

We use the JarKus data set as a reference since it is widely used to monitor coastal dynamics. We compare the JarKus transects in our study area with the trend inventory at the same locations and over the same three-year observation period.

After conversion of the coordinate systems we can place a JarKus transect on a point cloud collected on the same date and in this way verify, that the profiles and locations largely match. The transects are orthogonal to the *basic coastline* (BKL) and cover several cross sections of our grid structure. That is why we use an area of 10 m width to cover each of the two JarKus transects (see Fig. 2). Fig. 8 shows the JarKus transects at the location with ID 8225 together with a transect of a point cloud from the PLS data set acquired on the same day. We use this to match the JarKus transects with our data and validate the NAP elevation used for the calculation of the trend inventory. We are able to show the variability in the same locations as the transects in between measurement campaigns (as shown in Fig. 7).

However, in Fig. 8 it becomes clear that the JarKus transects cover a much larger area across shore, with large parts under water, while our study area only represents a small part of the transects. Any conclusions that we can draw out of our data set are therefore difficult to compare and match with the results on long-term coastal development from JarKus data. JarKus data is used for a variety of applications including the determination of the so-called *MKL-trend*, the trend of the momentary coastline (MKL), describing the current state of the coast compared to the previous years. A similar analysis with our data set would be based on a much smaller area, covering only the aeolian zone, as well as a relatively short time-span of three years. Therefore it proofs to be challenging to draw direct conclusions out of the statistics of the inventory of trends that are comparable to the MKL-trends based on JarKus measurements.

4.3. Categorisation of different topographic change processes

To show in more detail the potential of the information captured by our method, we discuss how three common process categories, a major storm, aeolian sand transport and bulldozer work, show up in our trend inventory. This demonstrates how our trend inventory can be used to analyse dynamics in between the yearly JarKus measurements with respect to different processes and at different time scales.

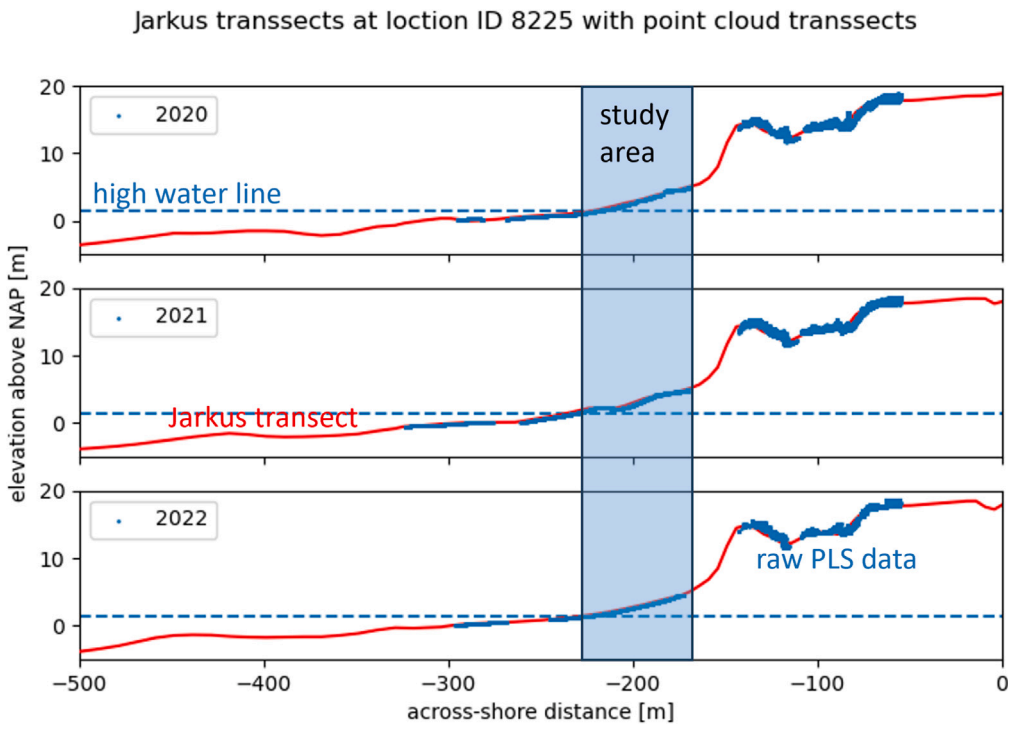

Fig. 8. Jarkus transects for 2020, 2021 and 2022 with the transect from a point cloud from raw PLS data acquired on the same day. The high water line and the borders of our study area are shown as well.

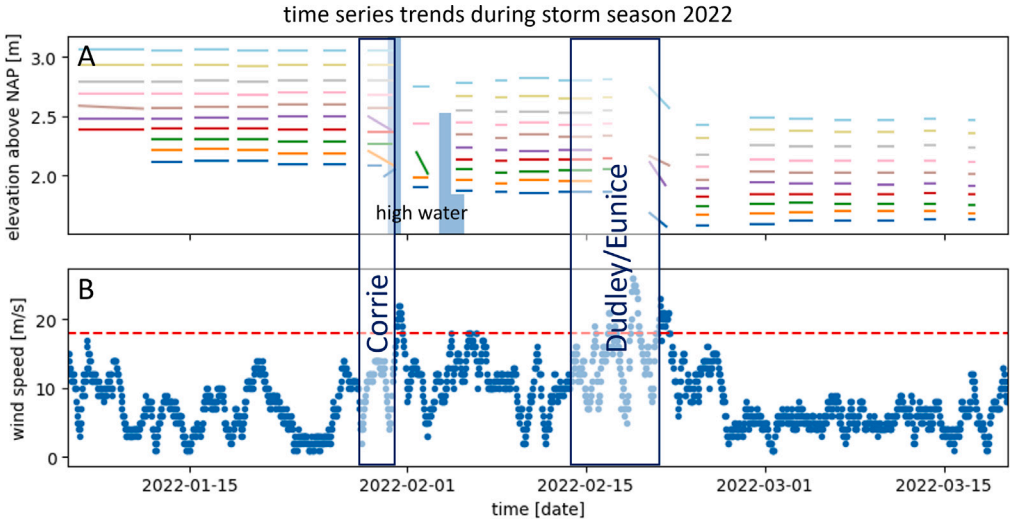

Fig. 9. A: Time series trends at 10 different grid cells indicated by 10 different colours in storm season 2021/2022 covering the major storms Corrie, Dudley and Eunice. B: Wind speed in the same time period. The dotted red line at 18 m/s wind speed provides the threshold for a 'major storm'. Occasions, where high water reaching up to the grid cells of the shown time series was recorded in our data set, are indicated with a blue bar.

Major storms

In Fig. 9 we show the effects of two major storms, Corrie and Eunice/Dudley in February 2022 exemplary at 10 grid cells. The example grid cells are located along a line perpendicular to the coast at $y = -55$ and $-215 \leq x \leq -197$ in steps of 2 m. The bottom panel shows wind speed at the same time with a threshold of 18 m/s as indication of a 'major storm'.

Storm Corrie would not register as a major storm according to our wind data collected at IJmuiden weather station. However, it occurred together with high tide resulting in an exceptional high water level which caused large parts of the beach to be temporarily flooded. In Fig. 9A, the blue bars indicate where the high water reached up to the location of the grid cells of the respective time series/fitted trends. Since all our study site is in the aeolian zone, flooding during tides happens mostly during storm conditions.

Eunice and Dudley were overlapping in time and caused very strong wind gusts but we did not register high water reaching our study area. Both storms caused some loss of data, either because of tides covering parts of the beach or through decreased data quality during strong winds. With the trends at different locations on the beach,we can clearly follow the erosion patterns that are caused by both storms. Possible reasons for erosion are either wave run up reaching the study area in between scans, high water covering the area during gaps in the data or aeolian sand transport. We record high water reaching the study area, when the smallest point cloud in one day shows the high water line within the study area. It is possible that these events happen

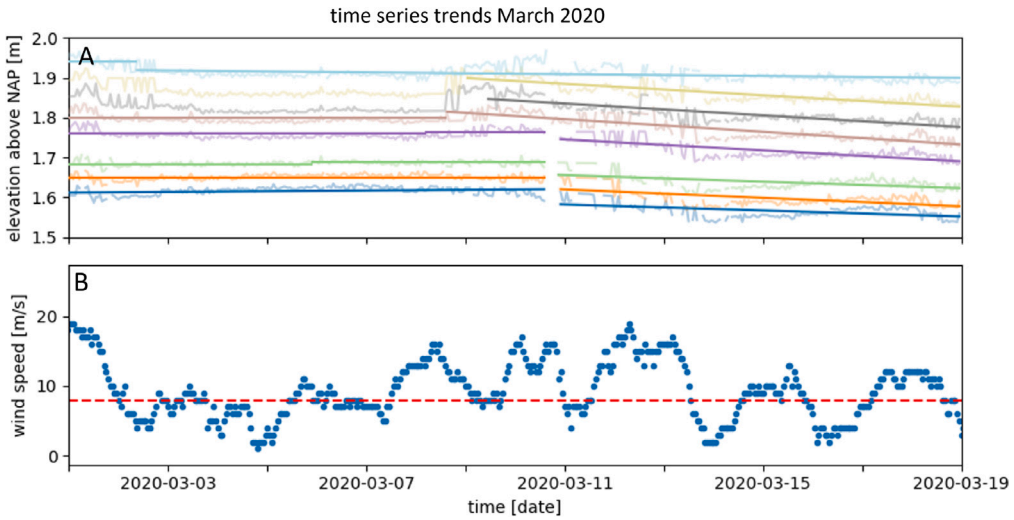

Fig. 10. A: Time series trends in March 2020 showing most likely occurrence of aeolian sand transport detected through the slow but continuous changes over several days together with wind speeds above 8 m/s (red dotted line, B). The original time series are shown together with each fitted trend.

without being recorded or that wave run up reaches the area while the high water line is just below the border of the study area.

Overall we estimate for the entire observation area a total positive volume change of 1667 m^3 for storm Corrie (with a duration of three days) and a total negative volume change of −3459 m^3 for Eunice/Dudley during six days. Our full observation area, compare Fig. 2, is roughly 41 000 m^2, thus resulting in an average gain of 4 cm per square meter during storm Corrie and an average loss of 8.4 cm per square meter during storms Eunice and Dudley. Most of the accretion is happening during data gaps, but we suspect that high water reaching the aeolian zone as well as wave run up are the main causes for accretion. We remark here that the impact of both storms was very different and even contrasting. The elevated water levels caused by Corrie are a likely explanation, despite the corresponding relatively lower wind speeds.

Aeolian sand transport

Additionally to large and sudden changes, the trend inventory is suitable for the observation of slow elevation changes developing during several hours or even days. For an example of aeolian sand transport we show time series trends at nine locations along a profile perpendicular to the coastline ($y = 150$ and $-206 \leq x \leq -198$) in steps of 1 m together with recorded wind speeds at that time (Fig. 10). The slow but continuously observed erosion over several days in combination with wind speeds higher than 8 m/s lead to the assumption that aeolian sand transport is the most likely cause of the elevation changes in these neighbouring grid cells. According to van Rijn (2022), dry sand with wind speeds of 8 m/s and higher provides the conditions for possible aeolian sand transport on the Dutch coast. We did not report on precipitation here, because precipitation varies locally and data from the weather stations at several 10 s of kilometres distance is not very accurate especially in coastal areas.

Fig. 10A shows how the slow erosion of a few centimetres over the course of 10 to 20 days is captured very well by the inventory of trends. Filtering the entire inventory of trends for partial time series with statistical significant rate of change, v, in the range $0\ m/h < v \leq 0.05\ m/h$, that last at least 6 h, provides an estimate of all the potential times and locations that aeolian sand transport caused changes in the sediment surface. This amounts to just under 395 000 partial time series with potential aeolian sand transport causing a deposition of sediment of about 1354 m^3 in our study area over three years time. This is equivalent to an average gain in elevation of 3.3 cm per square meter over three years.

Bulldozer works

Our study site is subject to frequent bulldozer works, compare Barbero-García et al. (2023) and Kuschnerus et al. (2022). Reasons for bulldozer works are mostly clearance of access paths and preventing and removing storm damage. Generally the beach is maintained frequently to facilitate recreational use. For the interpretation of the data and derived trends it is important to take the potential effects of bulldozer works into account. A prominent example found in our data set is the set up of a beach tent in test area 1 (see Fig. 2) next to the beach bar. Before the tent was set up in January 2020, a terrace was formed and the entire month saw frequent bulldozer activities in that area. We use this example to showcase how bulldozer works appears in our trend inventory. In Fig. 11 we show time series trends for 10 grid locations along the cross shore profile $y = 30$ and $-175 \leq x \leq -156$ in January 2020. In the bottom panel we show the total number of sudden changes per day (of 30 cm or higher) recorded in that area, which are most likely caused by bulldozer works. A list of these potential bulldozer activities was generated for Barbero-García et al. (2023), and is used here as reference indication.

We see in Fig. 11 that the bulldozer works interrupt the ongoing trends significantly. It takes almost two weeks until a regular situation with stable trends appears again. At the same time the bulldozer works lead to loss of data, due to occlusion and frequent interruption of time series. If there are too many gaps in a time series, a trend is not fitted by our method. The tent's set up after the bulldozer works, as well as sand piles can lead to occlusions in neighbouring grid cells.

4.4. Comparison of natural vs. anthropogenic processes

Bulldozer works are a common occurrence on the Dutch coast and coasts worldwide but their long-term effects on natural processes are difficult to study.

Here we use the list of instances most likely caused by bulldozer works collected for a previous study (Barbero-García et al., 2023), for a first assessment if a beach is affected by anthropogenic interventions and how many times these interventions occurred. We then chose two dedicated test areas (see Fig. 2), both of 760 m^2: Test area 1, where we suspect lots of anthropogenic influence (354 recorded incidences of possible bulldozer works) and Test area 2, with few bulldozer works (95 recorded incidences of possible bulldozer works) and therefore mostly natural influences but a similar location on the beach, close to the dunes.

For the comparison of these two areas we show in Fig. 12 the average rate of change of all fitted trends within the three year period

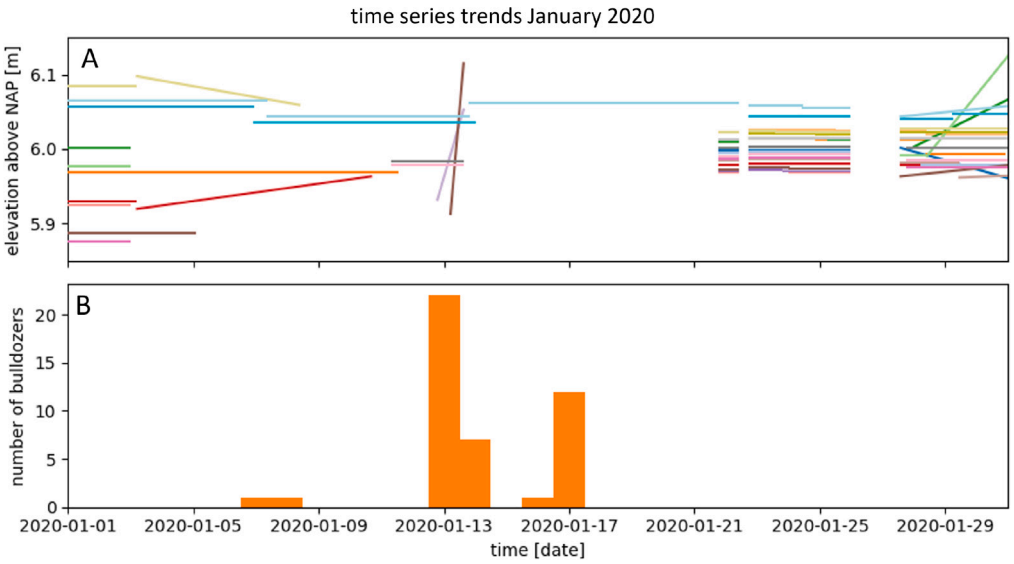

Fig. 11. A: time series trends for 10 grid locations in January 2020 showing the effects of bulldozer works in the middle of test area 1. B: Number of sudden changes per day. most likely caused by bulldozer works.

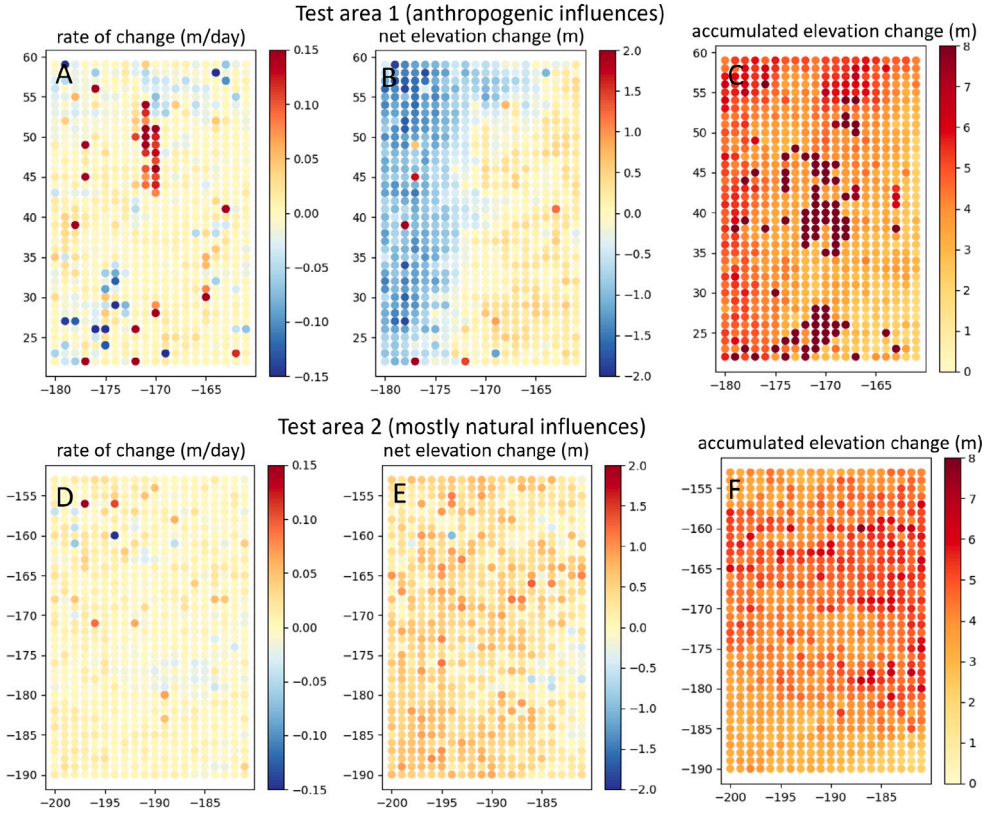

Fig. 12. Comparison of rates of change, net elevation change and absolute accumulated elevation change over the entire observation period in test area 1 and 2.

in that area (A and D) and the net elevation change that we derive out of all the fitted trends in the area (B and E). The accumulated elevation change (C and F) is calculated as the sum of all jumps that appear in the trend inventory and the recorded slow changes both as absolute values.

Test area 1, with lots of anthropogenic processes, shows lots of variability, see Fig. 12A–C. Over the entire observation period, the net volume change in that area was −257.5 m^3 with an average rate of change of 0.0071 m/day. Fig. 12B shows a clear pattern in both the yearly and entire period accumulated change from the dunes towards the sea, with erosion closer to the sea (west) and no change or some deposition closer to the dunes. The average rate of change however, Fig. 12A, reveals different patterns.

For comparison, Test area 2 is dominated by natural processes. In Fig. 12D–F we do not observe the patterns observed for Test area 1: Over the entire observation period the net volume change in Test area 2 was 272 m^3 with an average rate of change of 0.002 m/day. The overall accumulated net change as well as the average rate of change over the entire three-year period are visualised in Fig. 12E and F. This leads to the hypothesis, that more frequent anthropogenic human activity

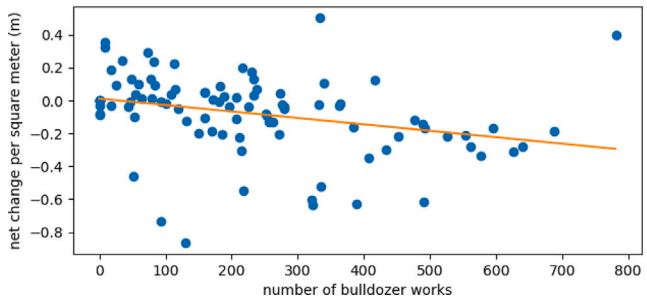

Fig. 13. Comparison of number of bulldozer works with net elevation change per square meter in the same area. The orange line shows a fitted trend.

occurs in areas where we also observe more erosion, compared to areas with less human influences.

To relate the amount of human activity (i.e. bulldozer works) in an area to the variability and erosion/deposition patterns in that area for our entire observation period, we compare the number of potential bulldozer works over the entire three year period to the variability, quantified as net change: with a moving window of 20 m length across-shore and 40 m length along-shore we collect for each window the number of bulldozer work instances and the net change over the three year period.

The result of this analysis is shown in Fig. 13, indicating a (small) negative correlation between net change and number of bulldozer works. The correlation coefficient of 0.3 supports this result. We therefore observe, that in our study site, most bulldozer works are happening in areas that were eroding during the observation period.

5. Discussion

We conclude that with the large and complex PLS data set, it is possible to observe interacting processes with unprecedented detail and complexity. The comparison with JarKus transects provided the opportunity to validate the elevation in the PLS data set. However, it also showed that a simple question, such as 'Is the coastline at a specific location retreating or advancing?' is not easily answered using our more complex data. For this question the JarKus data set is more suited to provide easily interpreted quantified answers. Generally speaking, we find a trade-off between the opportunity to research increasing complexity of a natural system vs. the need for clear and easy to communicate answers on major challenges of coastal engineering and monitoring. With the data from the trend inventory, we can provide general indicators of variability and also if there is generally a dominating trend of erosion or deposition. However, a direct comparison with the indicator of for example the MKL-trend is difficult.

The unique nature of the analysed data set lends itself to look for systematic analysis of coastal dynamics, which are mostly ruled by natural processes. The question if a 'heavy storm' causes more surface changes depending on the strength of the wind speed, was considered in this context. However, a consistent and systematic definition of a storm, based on one or two observed parameters, such as wind speed and wind direction proved to be difficult. As can be seen in our analysis (Section 4.3 and Fig. 9) two major storms present themselves differently in terms of wind speed as well as with their impact on the beach. We decided not to present an attempt at correlating for example sand volume change and wind speed in order to avoid a simplified presentation of a complex system of interacting natural forces and their effects. To improve this in similar future experiments, a weather station next to the laser scanner as well as wind meters in several locations on the beach would be recommended.

The PLS data set together with the inventory of trends provides many opportunities for more research. We showed in Section 4.3 how specific physical processes that cause elevation change at the sediment surface appear in the inventory of trends. Especially storm damage but also the more gradual and difficult to monitor aeolian sand transport appear with a clear pattern. Considering wind speed together with the trend inventory both can potentially be detected in a data set of a large long term study. There is also the opportunity to take a closer look at different regions and/or time scales. For example the analysis of seasonal changes in erosion/accretion patterns on the sediment surface could be interesting. However, accretion seems to happen mostly during storm conditions in our study area. Therefore the trend inventory appears not to be the ideal method for the detection and identification of accreting events. Adding additional means of observing the study area, for example through video cameras, could help to confirm the suspected causes of erosion/accretion during times of data loss and improve this point.

The acquisition of more PLS data sets could lead to the opportunity for the generation of training data for a possible supervised learning algorithm to detect these processes. We still consider our three year data set as insufficient for training an algorithm on the occurrence of a specific process, such as aeolian sand transport or a storm. But, we feel we have successfully demonstrated the possibility of identification of such processes in a PLS data set.

For the evaluation of the impact of anthropogenic activities, data from other locations and possibly specific long term experiments could be useful. The slight correlation between erosion and amount of bulldozer works that we show in Section 4.4, could be an indication, that frequent human interventions disturb the naturally occurring deposition of sand. Another interpretation could be that larger erosion requires more corrective bulldozer interventions. In any case it is important to consider the context, that all bulldozer works must be below 20 m^3 per transect of 1 m width, according to the Dutch regulations. This threshold is chosen in order to ensure that bulldozer works are in the same order of magnitude as natural processes and do not disturb them. However, the correlation that we show, could be an indicator that either more bulldozer works are happening than the regulation allows, or the threshold was based on a false assumption and there is indeed an impact of the frequent anthropogenic activities on natural processes. Both of these hypothesis need further research.

6. Conclusions

We analysed a three-year data set from permanent laser scanning with the help of hypothesis testing, to find statistically significant monotonic trends in elevation and reduce the complex data set to an inventory of trends. We furthermore showcased applications of the inventory of trends for the analysis of change patterns at the sediment surface in the aeolian zone of a Dutch sandy beach by answering four research questions:

- What elevation trends at the sediment surface can be derived from the PLS data set?
  We found about 380 000 thousand partial time series with statistically significant rates of change of 0.0027 m/day on average with an average duration of 158 h. We therefore show dynamics on the sediment surface that are difficult to study and to reveal with other techniques. Especially slowly developing elevation changes over longer periods of times (several days/weeks) and at cm level can be captured with our method.
- How do high resolution PLS data compare to yearly JarKus-data?
  The elevation from the PLS data set is validated at two locations of the JarKus transects at the day of acquisition of the JarKus data. Therefore our data set and method allows to show dynamics in between the measurement campaigns at these specific locations and in a small part of the JarKus transects. The comparison of long-term (up to 10 s of years) trends concerning the coast line proofs to be difficult. Our more complex and exhaustive data set,

on a smaller area does not allow to draw simple conclusions comparable to coastline trends from JarKus data, but shows dynamics that are missed by the yearly JarKus measurements.

- How can small and slow changes at the sediment surface be identified and quantified with PLS?
  We show that large elevation changes, for example caused by storms as well as slow, small-scale changes in elevation over longer periods of time can be identified and analysed with the inventory of trends. Especially small-scale, long term elevation changes, which are associated with aeolian sand transport are well captured within the inventory of trends. Anthropogenic activities such as bulldozer works can be found as well, but are easier detected with other methods, for example by considering sudden changes as presented by Barbero-García et al. (2023).
- How can the effect of anthropogenic activities on the dynamics at the sediment surface be analysed using PLS data?
  By comparing the number of bulldozer sightings in an area with the net elevation change in the same area and time frame we find a connection between erosion and bulldozer works with a correlation coefficient of 0.3. This leads to the hypothesis that bulldozer works negatively affect natural processes on the beach and might lead to more erosion. Further research is needed to confirm this hypothesis.

We presented a new method to gain information on change processes at the sediment surface on a sandy beach from a PLS data set. To extend this research we suggest comparison with similar data sets at other locations, as well as collection of more environmental variables (for example in situ wind speed and direction) in future similar experimental set-ups. The trend inventory is a tool that could potentially be used for many other applications and case studies, such as analysis of seasonal patterns in erosion/deposition, study of intertidal bar dynamics or dune growth.

CRediT authorship contribution statement

Mieke Kuschnerus: Writing – original draft, Visualization, Validation, Methodology, Formal analysis, Data curation, Conceptualization. **Sierd de Vries:** Writing – review & editing, Supervision, Methodology, Investigation, Funding acquisition, Conceptualization. **José A.Á. Antolínez:** Writing – review & editing, Supervision. **Sander Vos:** Writing – review & editing, Data curation. **Roderik Lindenbergh:** Writing – review & editing, Supervision, Project administration, Methodology, Conceptualization.

Declaration of competing interest

The authors declare that they have no known competing financial interests or personal relationships that could have appeared to influence the work reported in this paper.

Data availability

All data is published under http://dx.doi.org/10.4121/1aac46fb-7900-4d4c-a099-d2ce354811d2.v2. The dataset is referenced in the manuscript.

Acknowledgements

The authors would like to thank Grand Hotel Huis ter Duin for their cooperation. This research has been supported by the Netherlands Organization for Scientific Research (NWO, grant no. 16352) as part of the Open Technology Programme and by Rijkswaterstaat (Dutch Ministry of Infrastructure and Water Management).

References

Ackerley, D., Chandler, J., Bullard, J., 2016. Monitoring dune response to the east coast storm surge of 2013 using laser scanning and SfM photogrammetry. In: Coastal Management: Changing Coast, Changing Climate, Changing Minds. ICE Publishing, pp. 545–554. http://dx.doi.org/10.1680/cm.61149.545.

Anders, K., Lindenbergh, R.C., Vos, S.E., Mara, H., de Vries, S., Höfle, B., 2019. High-frequency 3D geomorphic observation using hourly terrestrial laser scanning data of a sandy beach. ISPRS Ann. Photogram. Remote Sens. Spat. Inf. Sci. IV-2-W5, 317–324. http://dx.doi.org/10.1016/j.isprsjprs.2019.11.025.

Barbero-García, I., Kuschnerus, M., Vos, S., Lindenbergh, R., 2023. Automatic detection of bulldozer-induced changes on a sandy beach from video using YOLO algorithm. Int. J. Appl. Earth Obs. Geoinf. 117, 103185. http://dx.doi.org/10.1016/j.jag.2023.103185.

Chang, L., Hanssen, R.F., 2016. A probabilistic approach for InSAR time-series postprocessing. IEEE Trans. Geosci. Remote Sens. 54 (1), 421–430. http://dx.doi.org/10.1109/TGRS.2015.2459037.

de Vries, S., Southgate, H., Kanning, W., Ranasinghe, R., 2012. Dune behavior and aeolian transport on decadal timescales. Coast. Eng. 67, 41–53. http://dx.doi.org/10.1016/j.coastaleng.2012.04.002.

Di Biase, V., Kuschnerus, M., Lindenbergh, R.C., 2022. Permanent laser scanner and synthetic aperture radar data: Correlation characterisation at a sandy beach. Sensors 22 (6), http://dx.doi.org/10.3390/s22062311.

Grabemann, I., Weisse, R., 2008. Climate change impact on extreme wave conditions in the North Sea: an ensemble study. Ocean Dyn. 58 (3), 199–212. http://dx.doi.org/10.1007/s10236-008-0141-x.

Hulskemper, D., Anders, K., Antolínez, J.Á., Kuschnerus, M., Höfle, B., Lindenbergh, R., 2022. Characterization of morphological surface activities derived from near-continuous terrestrial lidar time series. Int. Archiv. Photogram. Remote Sens. Spat. Inf. Sci. 48, 53–60. http://dx.doi.org/10.5194/isprs-archives-XLVIII-2-W2-2022-53-2022.

Intergovernmental Panel on Climate Change (IPCC), 2014. Climate change 2014 – impacts, adaptation and vulnerability: Part A: Global and sectoral aspects: Working group II contribution to the IPCC fifth assessment report. Vol. 1, Cambridge University Press, pp. 361–410. http://dx.doi.org/10.1017/CBO9781107415379.010, (Chapter Coastal Systems and Low-Lying Areas).

Killick, R., Fearnhead, P., Eckley, I., 2012. Optimal detection of changepoints with a linear computational cost. J. Amer. Statist. Assoc. 107 (500), 1590–1598. http://dx.doi.org/10.1080/01621459.2012.737745.

Koninklijk Nederlands Meteorologisch Instituut (KNMI), 2022. website. https://www.knmi.nl/nederland-nu/klimatologie/uurgegevens.

Kuschnerus, M., Lindenbergh, R., de Vries, S., 2023. Assessing sandy beach width variations on intertidal time scales using permanent laser scanning. In: 5th Joint International Symposium on Deformation Monitoring. JISDM 2022, Editorial Universitat Politècnica de València, pp. 113–119.

Kuschnerus, M., Lindenbergh, R., Lodder, Q., Brand, E., Vos, S., 2022. Deteching anthropogenic volume changes in cross sections of a sandy beach with permanent laser scanning. Int. Archiv. Photogram. Remote Sens. Spat. Inf. Sci. XLIII-B2-2022, 1055–1061. http://dx.doi.org/10.5194/isprs-archives-XLIII-B2-2022-1055-2022.

Kuschnerus, M., Lindenbergh, R., Vos, S., 2021. Coastal change patterns from time series clustering of permanent laser scan data. Earth Surf. Dyn. 9 (1), 89–103. http://dx.doi.org/10.5194/esurf-9-89-2021.

Kuschnerus, M., Lindenbergh, R., Vos, S., Hanssen, R., 2024. Statistically assessing vertical change on a sandy beach from permanent laser scanning time series. ISPRS Open J. Photogram. Remote Sens. 11, 100055.

Lindenbergh, R., Hanssen, R., 2003. Eolian deformation detection and modeling using airborne laser altimetry. In: IGARSS 2003. 2003 IEEE International Geoscience and Remote Sensing Symposium. Proceedings (IEEE Cat. No.03CH37477). Vol. 6, pp. 4113–4116. http://dx.doi.org/10.1109/IGARSS.2003.1295379.

Luijendijk, A., Hagenaars, G., Ranasinghe, R., Baart, F., Donchyts, G., Aarninkhof, S., 2018. The state of the world's beaches. Sci. Rep. 8 (1), 6641. http://dx.doi.org/10.1038/s41598-018-24630-6, Number: 1 Publisher: Nature Publishing Group.

Luijendijk, A.P., Ranasinghe, R., de Schipper, M.A., Huisman, B.A., Swinkels, C.M., Walstra, D.J., Stive, M.J., 2017. The initial morphological response of the sand engine: A process-based modelling study. Coast. Eng. 119, 1–14.

Maij-Weggen, J., 1990. Kustverdediging na 1990: Beleidskeuze voor de kustlijnzorg. Minist. Verkeer Waterstaat, 's-Gravenhage.

Poppema, D.W., Wijnberg, K.M., Mulder, J.P.M., Vos, S.E., Hulscher, S.J.M.H., 2021. The effect of building geometry on the size of aeolian deposition patterns: Scale model experiments at the beach. Coast. Eng. 168, 103866. http://dx.doi.org/10.1016/j.coastaleng.2021.103866.

Rijkswaterstaat - Dutch Ministery of Infrastructure and Water Management, 2022. URL: https://data.overheid.nl/en/dataset/17807-jarkusraaien.

Rijkswaterstaat, Rijksinstituut voor Kust en Zee, 2022. Report: Kustlijnkaart (document number 109949). URL: https://open.rijkswaterstaat.nl/open-overheid/onderzoeksrapporten/@133491/kustlijnkaarten-1992/.

Schipper, M.A.d., Vries, S.d., Ruessink, G., Zeeuw, R.C.d., Rutten, J., Gelder-Maas, C.v., Stive, M.J.F., 2016. Initial spreading of a mega feeder nourishment: Observations of the sand engine pilot project. Coast. Eng. 111, 23–38. http://dx.doi.org/10.1016/j.coastaleng.2015.10.011.

Schröder, D., Anders, K., Winiwarter, L., Wujanz, D., 2022. Permanent terrestrial LiDAR monitoring in mining, natural hazard prevention and infrastructure protection–Chances, risks, and challenges: A case study of a rockfall in Tyrol, Austria. In: Proceedings of 5th Joint International Symposium on Deformation Monitoring. JISDM, Valencia, http://dx.doi.org/10.4995/JISDM2022.2022.13649.

Schubert, J.E., Gallien, T.W., Majd, M.S., Sanders, B.F., 2015. Terrestrial laser scanning of anthropogenic beach berm erosion and overtopping. J. Coast. Res. 31 (1), 47–60. http://dx.doi.org/10.2112/JCOASTRES-D-14-00037.1.

Stive, M.J., Aarninkhof, S.G., Hamm, L., Hanson, H., Larson, M., Wijnberg, K.M., Nicholls, R.J., Capobianco, M., 2002. Variability of shore and shoreline evolution. Coast. Eng. 47 (2), 211–235. http://dx.doi.org/10.1016/S0378-3839(02)00126-6.

Truong, C., Oudre, L., Vayatis, N., 2020. Selective review of offline change point detection methods. Signal Process. 167, 107299. http://dx.doi.org/10.1016/j.sigpro.2019.107299.

Uphues, C.F.K., van IJzendoorn, C.O., Hallin, C., Pearson, S.G., van Prooijen, B.C., Miot da Silva, G., de Vries, S., 2022. Coastal aeolian sediment transport in an active bed surface layer: Tracer study and conceptual model. Earth Surf. Process. Landf. 47 (13), 3147–3162. http://dx.doi.org/10.1002/esp.5449.

van IJzendoorn, C.O., de Vries, S., Hallin, C., Hesp, P.A., 2021. Sea level rise outpaced by vertical dune toe translation on prograding coasts. Sci. Rep. 11 (1), 12792. http://dx.doi.org/10.1038/s41598-021-92150-x.

van IJzendoorn, C., Hallin, C., Cohn, N., Reniers, A., de Vries, S., 2023. Novel sediment sampling method provides new insights into vertical grain size variability due to marine and aeolian beach processes. Earth Surf. Process. Landf. 48 (4), 782–800.

van Rijn, L.C., 2022. A fully predictive model for aeolian sand transport, part 3: Verification and application of model for natural beaches. Coast. Eng. 171, 104051. http://dx.doi.org/10.1016/j.coastaleng.2021.104051.

van Wiechen, P., de Vries, S., Reniers, A., Aarninkhof, S., 2023. Dune erosion during storm surges: A review of the observations, physics and modelling of the collision regime. Coast. Eng. 186, 104383. http://dx.doi.org/10.1016/j.coastaleng.2023.104383.

Voordendag, A.B., Goger, B., Klug, C., Prinz, R., Rutzinger, M., Kaser, G., 2021. Automated and permanent long-range terrestrial laser scanning in a high mountain environment: Setup and first results. ISPRS Ann. Photogram. Remote Sens. Spat. Inf. Sci. V-2-2021, 153–160. http://dx.doi.org/10.5194/isprs-annals-V-2-2021-153-2021.

Vos, S., Kuschnerus, M., de Vries, S., Lindenbergh, R., 2023. 4D spatio-temporal laser scan dataset of the beach-dune system in Noordwijk, NL. http://dx.doi.org/10.4121/1aac46fb-7900-4d4c-a099-d2ce354811d2.v2, 4TU.ResearchData.

Vos, S., Lindenbergh, R., de Vries, S., 2017. CoastScan: Continuous monitoring of coastal change using terrestrial laser scanning. In: Proceedings of Coastal Dynamics 2017. Helsingør, Denmark, pp. 1518–1528.

Vos, S., van IJzendoorn, C., Lindenbergh, R., de Wulf, A., 2024. Asynchronous dune development on a Dutch urbanized beach due to buildings and other anthropogenic influences. Geomorphology preprint available at SSRN 4678320.

Vousdoukas, M.I., Ranasinghe, R., Mentaschi, L., Plomaritis, T.A., Athanasiou, P., Luijendijk, A., Feyen, L., 2020. Sandy coastlines under threat of erosion. Nat. Clim. Change 10 (3), 260–263. http://dx.doi.org/10.1038/s41558-020-0697-0.

Wijnberg, K.M., 2002. Environmental controls on decadal morphologic behaviour of the Holland coast. Mar. Geol. 189 (3–4), 227–247.

Winiwarter, L., Anders, K., Czerwonka-Schröder, D., Höfle, B., 2023. Full four-dimensional change analysis of topographic point cloud time series using Kalman filtering. Earth Surf. Dyn. 11 (4), 593–613.